

## Coal Fly Ash Waste, a Low-Cost Adsorbent for the Removal of Mordant Orange Dye from Aqueous Media

Teresa Rosa,<sup>a</sup> Angela Martins,<sup>b</sup> Maria T. Santos,<sup>a</sup> Teodoro Trindade<sup>a</sup> and Nelson Nunes<sup>\*a,b</sup>

<sup>a</sup>Área Departamental de Engenharia Química, Instituto Superior de Engenharia de Lisboa, Instituto Politécnico de Lisboa, R. Conselheiro Emídio Navarro, 1959-007 Lisboa, Portugal

<sup>b</sup>Centro de Química Estrutural, Faculdade de Ciências, Universidade de Lisboa, Campo Grande, 1749-016 Lisboa, Portugal

In this study, a coal fly ash material generated in a Portuguese coal thermal powerplant was tested as a low-cost adsorbent to remove dye molecules. Pre-treatment of the coal fly ash samples was not performed in order to reduce end use cost. Physical and chemical characterization revealed their inert nature and low effects lixiviation in aqueous media. Preliminary adsorption studies include adsorbent quantity, and adsorption kinetics. The adsorption studies focused on Mordant Orange 1 (MoI) dye, but two other molecules, Rhodamine B (RhB) and Methylene Blue (MeB) were also included for comparison reasons. The adsorption isotherms were tested with different models including Langmuir, Freundlich and modified Langmuir-Freundlich. The effect of temperature, pH and unburn carbon in the adsorption process were also studied. The results show that adsorption capacity of the coal fly ash occurs mainly due to electrostatic interactions between the adsorbent surface and the adsorbate, which depends on the pH of the aqueous media and the surface chemistry of the material, quantified by the point of zero charge,  $pH_{pzc}$ . These joint effects are responsible for the higher retention of MoI that is about 16 times higher, when compared to the other two molecules tested.

**Keywords:** coal fly ash, waste valorization, Mordant Orange 1, dyes, adsorption, aqueous media

### Introduction

In recent decades, the world has faced substantial challenges related to energy production driven mainly by health, environment and sustainability issues.<sup>1-3</sup> One of them is the large consumption of coal, which generates substantial quantities of coal fly ashes (CFA), the major solid waste from coal-fired thermal powerplants.<sup>4,5</sup> There are environmental and economic reasons to support the valorization of fly ashes: first, the minimization of disposal costs and landfill occupied areas, also contributing to circular economy. Second and not least, the financial return on sales of fly ashes or products produced from waste.<sup>5-7</sup> These and other reasons encourage the scientific community to look for new possible applications for CFA waste, taking advantage of relevant properties of this type of material. The chemical and physical characteristics of CFA are crucial in future applications and are strongly

dependent on the characteristics of the coal that originates the waste as well as its handling and storage.

Currently, only about 20% of the produced CFA is valued in some way, such as in soil amelioration, civil construction, ceramic industry, or environmental protection.<sup>8</sup> The rest is still disposed in landfills and/or lagoons with significant problems associated with transport, conditioning and monitorization in order to prevent soil and water contaminations.<sup>5</sup> In this context, it is imperative to find alternative applications for CFA, giving them a new valorization path from the perspective of circular economy principles.

Iyer *et al.*<sup>9</sup> reviewed several value-added uses of CFA beyond construction industry. The high silica content, as well as the presence of some alumina, makes CFA suitable as a starting material for the synthesis of zeolites, and several methodologies on the subject are available on the literature.<sup>10-14</sup> However, the synthesis procedure involves several steps, some of which quite energy demanding. A more direct application is the use as adsorbent in the

\*e-mail: amartins@deq.isel.ipl.pt; nnunes@deq.isel.ipl.pt

removal of contaminants in the gaseous and liquid phases, taking advantage of the porosity and chemical properties of CFA materials.<sup>6,7,15,16</sup>

Adsorption processes, comprising the preferential partitioning of substances from the gaseous or liquid phases onto the surface of a solid material, are widely used in industrial applications and in water and wastewater purification. The main properties that are responsible for the retention of the molecules at the solid surface are its porosity as well as the chemical surface groups present on the material. Activated carbons are, by far, the most common adsorbents,<sup>17,18</sup> however the adsorption behavior of alternative porous materials such as clays,<sup>19</sup> metal organic frameworks (MOFs),<sup>20</sup> ordered mesoporous carbons<sup>21</sup> or even modified egg shells<sup>22</sup> are also under exploration.

The use of CFA materials as adsorbents has been reported on the literature both for gas and liquid phase adsorption. Regarding the removal of atmospheric contaminants, Lu *et al.*<sup>23</sup> successfully reported the adsorption of NOx pollutants and found that the amount of unburnt content remaining in the fly-ash was able to activate and improve the adsorption behavior. The CFA also revealed enormous potential for carbon capture and storage.<sup>24</sup> In water and wastewater treatment the range of possible applications is massive,<sup>25</sup> for instance, the adsorption of heavy metals such as mercury,<sup>26</sup> arsenic,<sup>27</sup> lead,<sup>28</sup> nickel,<sup>16,29</sup> cadmium,<sup>30</sup> chromium<sup>31</sup> and others<sup>32-34</sup> was recently reported. The use of CFA as adsorbent of other chemical species such as fluorides,<sup>35</sup> sulfates,<sup>3</sup> urea,<sup>36</sup> and phenol<sup>37</sup> has been also successfully tested. The removal of colored matter from wastewaters, particularly industrial dyes, using CFA has also been widely explored.<sup>38,39</sup> Despite the low dye concentration in coloring processes the intensive use of these substances may lead to toxic and carcinogenic effects since they tend to accumulate in the environment.<sup>40</sup> In several studies regarding the adsorption of both cationic and anionic dyes by fly ashes, authors concluded that the removal efficiency of dye molecules are closely linked to the textural and chemical

properties of the CFA<sup>41</sup> as well as the aqueous media characteristics such as pH and temperature.<sup>42,43</sup>

The aim of this work is to evaluate the behavior of raw coal fly ashes in the removal of dyes from synthetic industrial wastewaters; CFA were used without further treatment to reduce the processing costs. The study is focused on a less studied dye, Mordant Orange 1 (C<sub>13</sub>H<sub>9</sub>N<sub>3</sub>O<sub>5</sub>) and for a comparison purposes data from other two dyes, Rhodamine B (C<sub>28</sub>H<sub>31</sub>ClN<sub>2</sub>O<sub>3</sub>) and Methylene Blue (C<sub>16</sub>H<sub>18</sub>ClN<sub>3</sub>S) is also included. Variables such as pH, temperature, and adsorbent dosage, were experimentally tested in order to assess the effect of each parameter in the adsorption process.

## Experimental

### Adsorbent sample and dyes

The coal fly ash (CFA) waste, used as adsorbent, was generated in a Portuguese thermal powerplant, which burns a bituminous coal type from Colombia. The flue gas treatment method comprises the catalytic denitrification with ammonia, particle emission reduction with electrostatic precipitator and desulfurization with limestone. The studied CFA samples were collected from the powerplant storage silos containing ashes from the electrostatic precipitators.

The CFA samples were experimentally tested without further treatment. The dyes used as adsorbates were: Mordant Orange 1 (Mo1; CAS No. 2243-76-7) and Rhodamine B (RhB; CAS No. 81-88-9) purchased from Sigma-Aldrich (St. Louis, USA) and Methylene Blue (MeB; CAS No. 61-73-4) acquired from Merck (Darmstadt, Germany). All dyes were used without further purification. Figure 1 shows the chemical structures and selected properties of the tested dyes.

### Characterization of CFA materials

The elemental analysis (used to quantify the content in

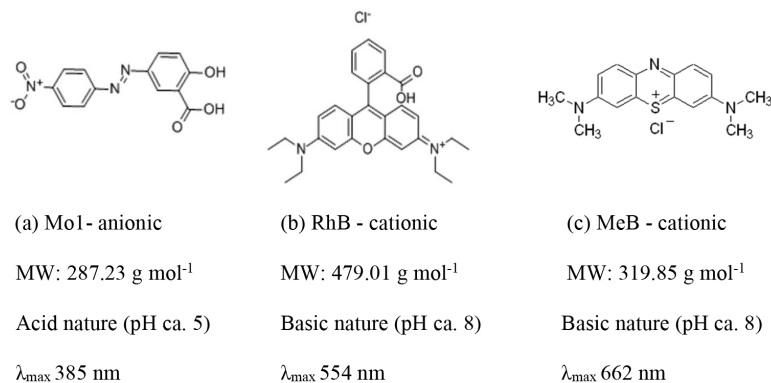


**Figure 1.** Chemical structures and properties of the tested dyes.

carbon, hydrogen, nitrogen and sulfur) and the proximate analysis (moisture, volatile compounds and ash content) were performed based on ASTM D1762-84.<sup>44</sup>

The quantification of inorganic matter was determined by inductively coupled plasma atomic emission spectrometry (ICP-AES) using the Horiba Jobin (Kyoto, Japan) Yvon analyzer (Ultima model). CFA samples were previously submitted to acid digestion in closed vessels in a Milestone Ethos microwave 1600 (Soriso, Italy) according to the European Standard 15290.<sup>45</sup>

Unburnt carbon content of CFA was quantified by sample weight loss on heating to a high temperature (950 °C). Leaching tests were also performed, using a liquid to solid ratio of 10 L kg<sup>-1</sup>.<sup>46</sup>

The X-ray diffraction pattern was obtained in a Pan'Analytical diffractometer, PW3050/60X'Pert PRO, (Almelo Netherlands) operating at 40 kV/30 mA, using Cu K $\alpha$  radiation in a wide-angle region from 5 to 80° on 2 $\theta$  scale and 0.017° step size.

A Brüker Vertex, 70 FTIR spectrometer (Billerica, MA, United States) was used in the Fourier transform infrared spectroscopy (FTIR) assays, the sample pellets were prepared by thoroughly mixing in an agata mortar, CFA with KBr in a ratio of 1:100. The spectral wavelength covered a range of 500 to 4000 cm<sup>-1</sup> with 4 cm<sup>-1</sup> resolution.

The morphology of the CFA solid particles was examined through images obtained in a scanning electron microscope (SEM) JEOL JSM 840 (Akishima, Japan).

Textural properties were studied by molecular nitrogen adsorption isotherms at a temperature of 77 K using a tailor-made volumetric apparatus with an assembly of two vacuum pumps: a rotary (RV5) and a diffusion (Diffstak MK2), both from Edwards (Irvine, California, USA). The apparatus is made of a customized glass vacuum line lubricated and vacuum sealed taps (Springham) equipped with two pressure sensors (Barocel 600 AB) and Penning (AIM-S-NW225) from Edwards. Prior to the adsorption measurements the samples (about 50 mg) were degassed under primary vacuum at 573 K for 2 h in a tubular oven, Eurotherm 2416, (Madrid, Spain). After cooling, the cell containing the sample was immersed in liquid nitrogen and then the admissions of N<sub>2</sub> (gas) were made at successive relative pressures until reaching a relative pressure higher than 0.95. The specific surface was calculated following the Brunauer-Emmet-Teller (BET) method.<sup>47</sup>

To complement textural characterization of the CFA, particle size distribution assays were performed through laser beam diffraction (Mastersizer 3000) under dry test conditions (air flux).

The point of zero charge (pH<sub>pzc</sub>) of the CFA was determined following the procedure described by

Prahas *et al.*<sup>48</sup> In brief, 150 mg of a CFA sample was added to 50 mL of 0.01 M solution of NaCl previously bubbled with N<sub>2</sub>, to release the dissolved CO<sub>2</sub>, until it reached a stable pH value, measured by a pH meter, Crison GLP22 (Barcelona, Spain). The CFA suspension was left for 24 h in a close environment at 25 °C and constant stirring. The test pH was adjusted within a range of 2-12 for each essay using HCl or NaOH solutions.

#### Adsorption kinetics and isotherms

To evaluate the efficiency as adsorbent, 100 mg of CFA was accurately weighted and placed in 50 mL stoppered flasks. Then, a volume of 40 mL of dyes solutions was added to the flasks and stoppered. The flasks were immersed in a thermostatic bath at 30 °C, Julabo MP (Seelbach, Germany) which was placed on a multi-position magnetic stirrer, Multimatic 9-S, Selecta (Cham, Switzerland). In the case of kinetic studies aliquots of the solution (about 1 mL) were then taken with established time intervals using the same dye concentration. In isotherm studies the aliquots (about 1 mL) were collected after reaching equilibrium time for each dye concentration. In both cases the solutions were analyzed in a double beam absorption spectrophotometer, Jasco V530 (Tokyo, Japan) using deionized water as reference and standard quartz cell of 2- and 10-mm optical length. The CFA powder was separated from dye solution using a membrane filter (Millipore Durapore 0.45  $\mu$ m HV). The spectrophotometer calibration curve was built using standard dye solutions and readings at maximum absorbance for each dye, Figure 1. The dye solutions were prepared within the appropriate concentration range to achieve absorbances comprised between 0.05 and 1.5, to obey Beer-Lambert law. Each data point resulted from an average of at least three individual aliquots/scans assuring a standard deviation below 5%. The specific amount of dye removed  $q_t$  (mg g<sup>-1</sup>) at a certain time  $t$ , was calculated according to equation 1.

$$q_t = \frac{C_0 - C_t}{1000 \times W} \times V \quad (1)$$

where  $C_0$  and  $C_t$  (mg L<sup>-1</sup>) corresponds respectively to the initial dye concentration and the concentration measured after a certain time,  $V$  (L) is the volume of solution and  $W$  is the mass of the CFA sample (g).

The adsorption isotherm equilibrium assays were performed according to the procedure described above. After 2 h of contact between the dye solutions and the CFA samples, the equilibrium is reached between the two

phases. As the experimental absorbance values only allow to obtain the concentration of dye that remained in solution, the amount of adsorbed dye,  $q_e$ , ( $\text{mg g}^{-1}$ ) is calculated using equation 2, where  $C_e$  ( $\text{mg L}^{-1}$ ) is the dye equilibrium concentration.

$$q_e = \frac{C_0 - C_e}{1000 \times W} \times V \quad (2)$$

The relation between the amount of dye adsorbed on the CFA and the equilibrium concentration of the dye solution can be described by different adsorption models. The Langmuir model is the most used to obtain characteristic parameters of adsorbate-adsorbent interactions in liquid phase, assuming the formation of a monolayer at the surface of the adsorbent material.<sup>31,32</sup> The model can be mathematically described by equation 3.

$$q_e = \frac{q_m \times K_L \times C_e}{1 + K_L \times C_e} \quad (3)$$

where  $q_m$  is the adsorption capacity of the monolayer ( $\text{mg g}^{-1}$ ) and  $K_L$  is the Langmuir constant ( $\text{L mg}^{-1}$ ), which can be related with the affinity between the adsorbent and the adsorbate.  $K_L$  and  $q_m$  are characteristic parameters of each adsorbent/adsorbate system.

Another two-parameter equation is the Freundlich model (equation 4).

$$q_e = K_F C_e^{1/n} \quad (4)$$

where  $K_F$  is the Freundlich constant ( $\text{mg}^{1-1/n} \text{L}^{1/n} \text{g}^{-1}$ ) representing the adsorption capacity, and  $1/n$  is related to the adsorption intensity or surface heterogeneity (favorable with values between 0 and 1).

A model having a higher complexity includes the modified Langmuir-Freundlich, a three-parameter model which combines the two previous models (equation 5).

$$q_e = \frac{q_m \times K_{MLF} \times C_e^{1/n}}{1 + K_{MLF} \times C_e^{1/n}} \quad (5)$$

where  $K_{MLF}$  is a model constant ( $\text{L mg}^{-1}$ ) and the value of  $1/n$  is a normalized parameter between 0 and 1.

Like isothermal modeling, the kinetic study of the adsorption process also provides physical-chemical information. The pseudo first order kinetic of Özacar and Sengil<sup>49</sup> may be expressed according to equation 6.

$$\ln(q_e - q_t) = \ln q_e - k_{p1} \times t \quad (6)$$

where  $k_{p1}$  is a kinetic constant of pseudo-first order ( $\text{min}^{-1}$ ) and  $t$  the time (min).

The pseudo-second order kinetics of Ho and McKay<sup>50</sup> may be represented by equation 7.

$$\frac{t}{q_t} = \frac{1}{k_{p2} \times q_e^2} + \frac{1}{q_e} \times t \quad (7)$$

where  $k_{p2}$  is a kinetic constant of pseudo-second order ( $\text{g (mg min)}^{-1}$ ).

## Results and Discussion

### Characterization of coal fly ash (CFA)

The proximate analysis data are presented in Table 1.

**Table 1.** Proximate analysis of coal fly ash

Proximate analysis / (% m/m)	
Fixed carbon	2.39 ± 0.16
Volatiles	3.40 ± 0.12
Ash	94.13
Moisture	0.07 ± 0.03

The proximate analysis data show a low content in moisture and volatile matter (Table 1), indicating an almost complete coal burn, as energetically desirable for a coal feedstock in a thermal powerplant.

The mineral content of CFA was examined, as well as the leaching properties of CFA in contact with aqueous media. The elements were divided in two groups according to their relative content. As expected, the major components (higher than 1000  $\text{mg kg}^{-1}$ ) are aluminum, iron, and silicon, being aluminium the most abundant element (Figure 2a). The minor components include sodium, manganese, and zinc, among others (Figure 2b).

The leaching of CFA components in aqueous media is an important parameter to evaluate their compatibility as adsorbent material, a low component release to aqueous environments being an advantage. There are many factors that can affect the leaching capacity, the most important the fly-ash composition and solution pH.<sup>51</sup> Figure 3 depicts the experimental concentration of elements in the aqueous leachate divided by their relative abundance. In this study, following the normalized procedure reported above, the elements that experienced leaching more significantly were Ca, Mg and K (Figure 3), but in very small amounts that can be considered environmentally safe.<sup>52</sup> Therefore, it is concluded that CFA can be safely used in aqueous medium without significant release of harmful elements through lixiviation.

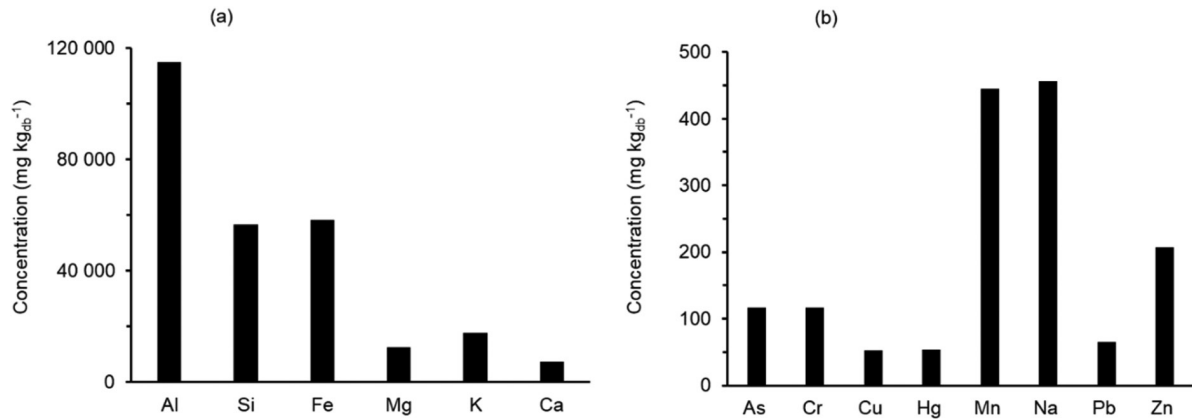


**Figure 2.** Metal elements content in the CFA (dry basis). (a) Major components and (b) minor components.

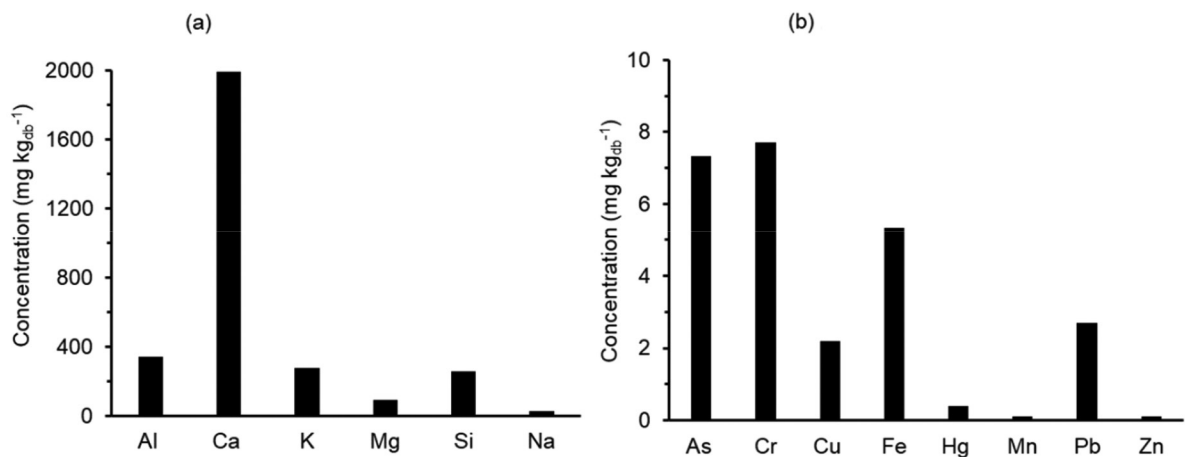


**Figure 3.** Aqueous leachate content in inorganic elements (dry base). (a) Major components and (b) minor components.

The X-ray diffraction was performed in order to identify crystalline phases in the CFA. The diffractogram presented on Figure 4 show the predominance of two crystalline phases: quartz (Q) with an estimated relative percentage of about 77.9% and mullite (M) around 8.0% which can be present in two stoichiometric forms,  $3\text{Al}_2\text{O}_3 \cdot 2\text{SiO}_2$  or  $2\text{Al}_2\text{O}_3 \cdot \text{SiO}_2$ . It was also possible to identify the presence of a small amount of magnetite (Mt).<sup>36,39,40</sup>

Infrared spectroscopy analysis (FTIR) was performed to investigate the nature of functional groups present on CFA. The spectra (not shown) present the main characteristic band located around  $1705 \text{ cm}^{-1}$ . This band is attributed to the asymmetrical elongation mode Si–O–Si or Al–O–Si. Another important band is located around  $3441 \text{ cm}^{-1}$  that is ascribed to Si–OH bonds and water molecules adsorbed to the surface of the ash.<sup>53</sup>

The SEM images presented in Figure 5 allows to perceive the morphology of CFA particles.

The images show a large number of spherical particles which can be identified as cenospheres, and pleuroospheres which are larger diameter structures with enclosing sub-microspheres or other mineral fragments. The size and shape

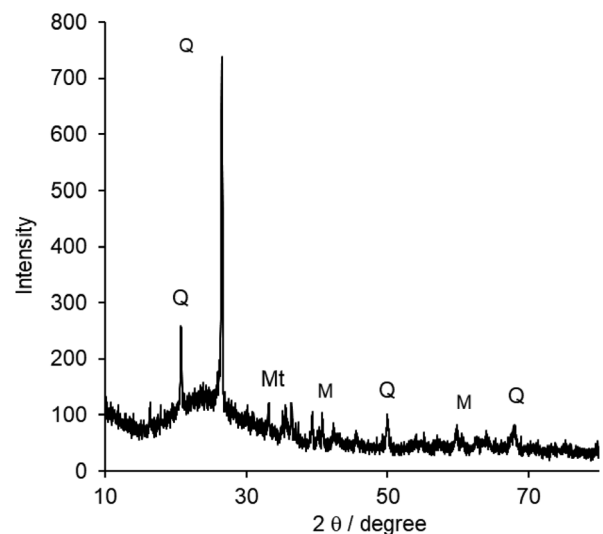


**Figure 4.** XRD diffraction pattern of coal fly ash. Identified phases: M: mullite; Q: quartz; Mt: magnetite.

of these spheres depends on the expansion of CO and  $\text{CO}_2$  gases in coal combustion furnaces. Other structures like glassy fragments, carbon blocks and spongy grains (Figure 5b) can be also found in CFA.<sup>42,54</sup>

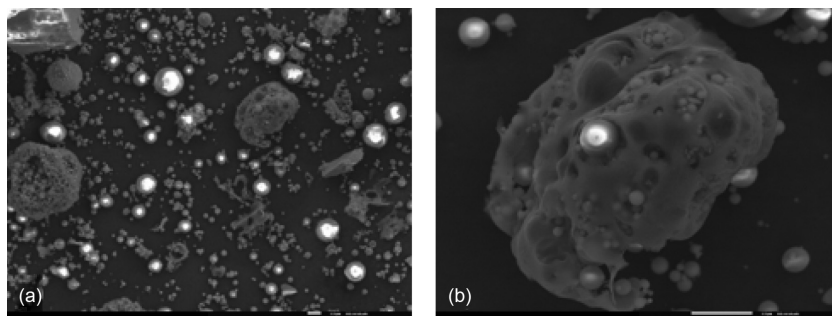


**Figure 5.** SEM images of the coal fly ash at magnification: (a)  $\times 100$  and (b)  $\times 1800$ .

Textural characterization of CFA was performed through low temperature molecular nitrogen adsorption isotherms and complemented by particle size distribution analysis. The application of BET model to the adsorption isotherm data of CFA indicates a specific surface area of  $13.2 \text{ m}^2 \text{ g}^{-1}$ . This value corresponds to a much lower textural level when compared to classic adsorbent materials like activated carbons. The granulometric distribution revealed the existence of particle diameters ranging from  $0.5$  to  $10 \mu\text{m}$ . Both textural and granulometric particle distributions of the tested CFA are in accordance to the ones reported in literature concerning similar materials.<sup>55-57</sup>

The interaction of the species with the surface of CFA strongly depends on the relationship between the pH of the species in aqueous media and the surface charge of the fly-ash material, quantified the point of zero charge  $\text{pH}_{\text{PZC}}$ , which for the tested CFA is about 11. The balance between the pH of a certain molecule in solution and the  $\text{pH}_{\text{PZC}}$  is fundamental since it can predict the behavior of an adsorbate/adsorbent system. If the solution pH is above the  $\text{pH}_{\text{PZC}}$  than the adsorbent surface will become negatively charged and will favor the removal of cations. On the other hand, if the pH of the solution is below the  $\text{pH}_{\text{PZC}}$  of the adsorbent material it will become positively charged and will attract anionic species.<sup>47,48</sup>

#### Preliminary adsorption studies

With the purpose of optimizing the experimental conditions for the adsorption studies, preliminary assays using MoI dye as adsorbate were done. First studying the adsorbent dosage effect, and afterwards the kinetic experiments, which also help to establish the equilibrium time.

#### Effect of adsorbent dosage

The effect of adsorbent dosage was evaluated using different quantities of CFA in contact with a MoI dye solutions with equal concentration. This preliminary study

evaluates the adequate quantity to be used in the subsequent adsorption studies. Figure 6 shows the profile of the MoI concentration that remains in solution after contacting with increasing amount of CFA for 1 h, at  $30^\circ\text{C}$ .

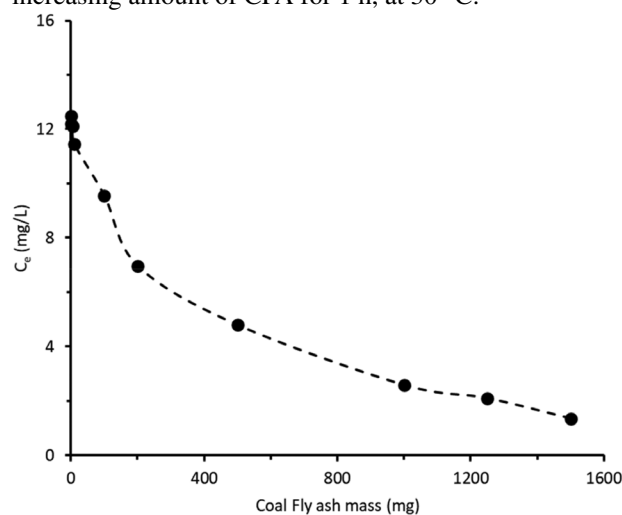


**Figure 6.** Concentration of MoI as a function of CFA mass at  $30^\circ\text{C}$  for 1 h.

As observed, for small amounts of CFA there is a sharp decrease in the MoI concentration as the amount of adsorbent increases, which becomes less pronounced for CFA quantities higher than  $1000 \text{ mg}$ . In further adsorption studies the amount of CFA was kept as  $100 \text{ mg}$ , clearly higher than the amounts used in adsorption studies using classic adsorbents like activated carbons where  $10$  to  $50 \text{ mg}$  are generally used. But, it must be bear in mind that, in this case, the final goal is the valorization of a residue.

#### Kinetic studies

The effect of contact time on the adsorption capacity of CFA was studied using MoI as adsorbate. The experimental profile of dye concentration with time is displayed in Figure 7.

Data shows a fast initial decrease of MoI concentration until reach an almost constant value after  $15 \text{ min}$ . Thus, in further studies the equilibrium time was considered  $15 \text{ min}$ .

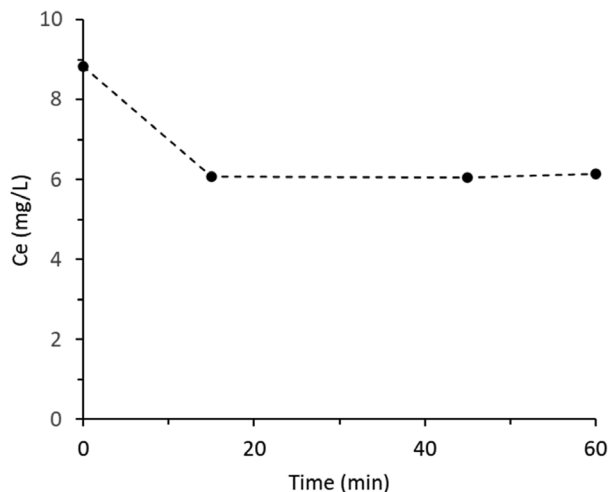


**Figure 7.** Concentration of Mo1 as a function of contact time at 30 °C.

To investigate the kinetics of the adsorption process pseudo first-order and pseudo-second order kinetic models were applied to the adsorption of Mo1 and the respective plots according to equations 3 and 4 are displayed in Figure 8.

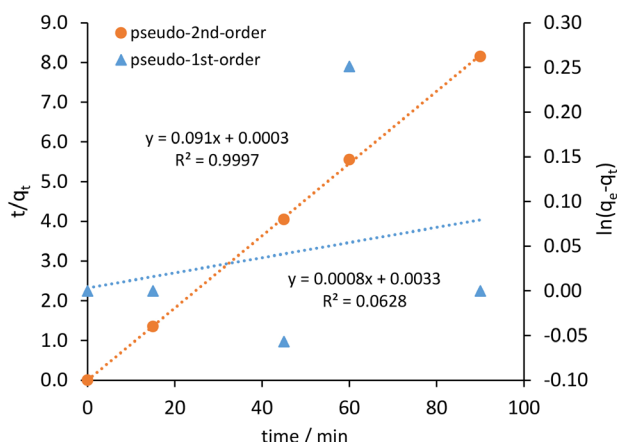


**Figure 8.** Pseudo-first order ( $\Delta$ ) and pseudo-second-order ( $\circ$ ) adsorption kinetics plots for Mo1 dye.

As observed, for the adsorption of Mo1 dye in CFA the best fitting kinetic model is the pseudo-second-order model. Other studies regarding the adsorption of distinct dye molecules also obey to a pseudo-second-order kinetic model.<sup>24,34,58</sup> Accordingly, it can be assumed that the other two molecules studied in this work also obey a pseudo-second-order adsorption kinetic.

The kinetic study also allowed to establish the equilibrium time of 2 h in the subsequent adsorption isotherm experiments. The chosen time largely exceeded the estimated equilibrium time from Figure 7, but assured the equilibrium condition was met for each experiment and tested dye.

## Adsorption isotherms

Adsorption isotherms were performed for the three dyes, Mordant Orange 1 (Mo1), Rhodamine B (RhB) and Methylene Blue (MeB), using the adsorbent dosage and contact time previously defined. The adsorption studies were made at three different temperatures 20, 30 and 40 °C, to evaluate the influence of temperature on the adsorption yield. Figure 9 shows the experimental adsorption isotherms.

All isotherms are positive, regular and concave in relation to the abscissa axis (dye concentration). However, for all temperatures the Mo1 isotherms show a significant higher amount of adsorbed dye when compared with the other two dyes, suggesting higher adsorption capacity for Mo1. Additionally, the isotherm plots also show that adsorption/desorption equilibrium maximum is reached at low dye concentration for RhB and MeB dyes.

Langmuir, Freundlich and the modified Langmuir-Freundlich adsorption models were applied to the experimental data. The model's adsorption parameters and the associated uncertainties are presented in Tables 2, 3 and 4.

Despite the apparent best fit of the modified Langmuir-Freundlich (high values of determination coefficients,  $R^2$ ), this three-parameter model from a statistical point is always less significant when compared with other models which have higher  $F$  values and lower parameters uncertainties. It was possible to confirm that the Langmuir model is the one that best describes the studied adsorption process in accordance with previous studies of Astuti *et al.*<sup>41</sup> which related better fits to the Langmuir model to low unburnt carbon on fly ashes, as is the case of our sample (5.3%). This fact also suggests the formation of an adsorbate monolayer at the surface of the adsorbent material.<sup>17</sup>

Bibliographic data for the adsorption of Mo1 in coal fly ash is very scarce, so no direct comparison results are presented, the only available data for different textural and surface chemistry materials. On the other hand, there are several studies concerning RhB or ReB in the adsorption with untreated CFA from thermal powerplants.<sup>17,25,41,49,59</sup> Despite a direct comparison between different CFA can be unreliable (due to differences in the coal composition and power plant processes) it is relevant to compare the maximum monolayer adsorption capacities (Langmuir adsorption isotherm). Table 5 depicts some of these literature results and regardless of the values variability they are in the same order of magnitude.

## Temperature effect

The effect of temperature on dye removal can be evaluated through the Langmuir equilibrium constants.

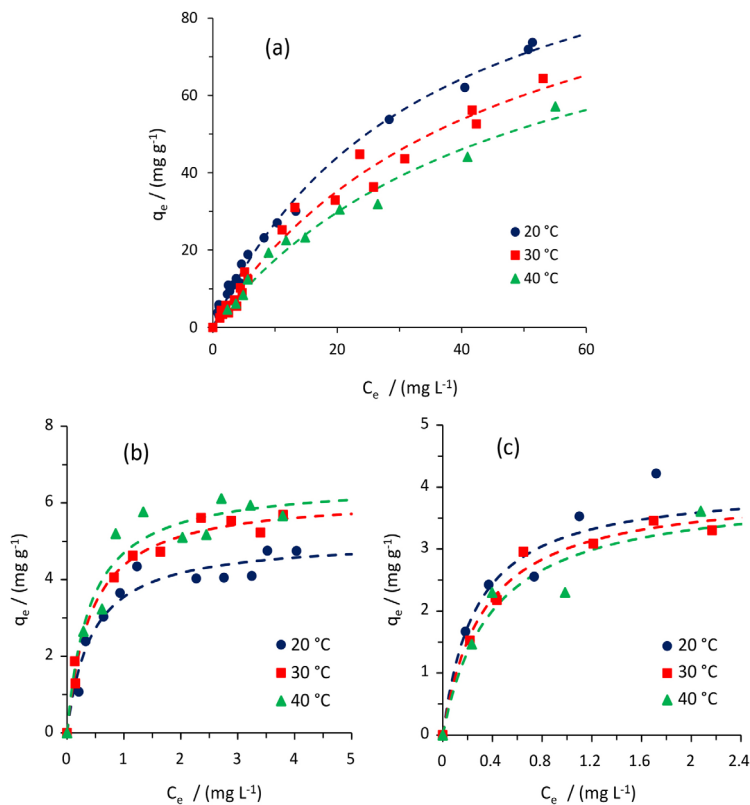


**Figure 9.** Adsorption isotherms on CFA at 20, 30 and 40 °C of (a) Mo1, (b) RhB and (c) MeB. The fitting curves are the Langmuir model.

**Table 2.** Adsorption parameters obtained by the application of Langmuir adsorption model

Langmuir isotherm model						
Adsorbate	Temperature / °C	$q_m / (\text{mg g}^{-1})$	$K_L / (\text{L mg}^{-1})$	$R^2$	$\sigma^2$	$F$
Mo1	20	$119.2 \pm 5.4$	$0.029 \pm 0.002$	0.969	1.840	3047
	30	$113.2 \pm 11.5$	$0.022 \pm 0.004$	0.983	2.732	1152
	40	$101.1 \pm 12.1$	$0.021 \pm 0.004$	0.982	2.389	553
RhB	20	$5.1 \pm 0.3$	$2.3 \pm 0.5$	0.952	0.356	179
	30	$6.2 \pm 0.2$	$2.4 \pm 0.9$	0.985	0.239	662
	40	$6.6 \pm 0.4$	$2.5 \pm 0.8$	0.935	0.524	116
MeB	20	$4.0 \pm 0.5$	$3.8 \pm 2.0$	0.895	0.484	42
	30	$3.98 \pm 0.02$	$3.1 \pm 0.5$	0.984	0.158	364
	40	$3.95 \pm 0.07$	$2.5 \pm 1.1$	0.935	0.389	43

$q_m$ : adsorption capacity;  $K_L$ : equilibrium constant;  $R^2$ : determination coefficient;  $\sigma^2$ : standard deviation fit;  $F$ : Fisher-Snedecor parameter; Mo1: Mordant Orange 1; RhB: Rhodamine B; MeB: Methylene Blue.

**Table 3.** Adsorption parameters obtained by the application of Freundlich adsorption model

Freundlich isotherm model						
Adsorbate	Temperature / °C	$K_F / (\text{mg}^{1-1/n} \text{L}^{1/n} \text{g}^{-1})$	$n$	$R^2$	$\sigma^2$	$F$
Mo1	20	$5.5 \pm 0.3$	$1.52 \pm 0.03$	0.995	1.633	3873
	30	$3.8 \pm 0.5$	$1.40 \pm 0.07$	0.976	3.223	822
	40	$3.7 \pm 0.4$	$1.47 \pm 0.07$	0.985	2.192	659
RhB	20	$3.2 \pm 0.2$	$3.5 \pm 0.7$	0.901	0.512	82
	30	$3.9 \pm 0.2$	$3.2 \pm 0.4$	0.945	0.460	172
	40	$4.4 \pm 0.3$	$4.0 \pm 1.0$	0.903	0.654	74
MeB	20	$3.0 \pm 0.2$	$3.8 \pm 1.4$	0.872	0.534	34
	30	$2.8 \pm 0.1$	$3.4 \pm 0.6$	0.958	0.254	138
	40	$2.6 \pm 0.2$	$2.8 \pm 0.6$	0.956	0.319	66

$K_F$ : Freundlich constant;  $n$ : heterogeneity factor;  $R^2$ : determination coefficient;  $\sigma^2$ : standard deviation fit;  $F$ : Fisher-Snedecor parameter; Mo1: Mordant Orange 1; RhB: Rhodamine B; MeB: Methylene Blue.

**Table 4.** Adsorption parameters obtained by the application of modified Langmuir and Freundlich adsorption models

Modified Langmuir-Freundlich isotherm model							
Adsorbate	Temperature / °C	$q_m / (\text{mg g}^{-1})$	$K_{\text{MLF}} / (\text{L mg}^{-1})$	$n$	$R^2$	$\sigma^2$	$F$
Mo1	20	222.9 ± 69.2	0.021 ± 0.005	1.26 ± 0.08	0.996	1.416	2581
	30	109.2 ± 27.4	0.023 ± 0.004	1.0 ± 0.1	0.983	2.802	547
	40	266 ± 386	0.012 ± 0.014	1.3 ± 0.3	0.985	2.267	308
RhB	20	4.5 ± 0.2	5.4 ± 2.6	0.6 ± 0.1	0.966	0.318	114
	30	6.2 ± 0.4	2.53 ± 0.7	1.0 ± 0.1	0.985	0.252	298
	40	6.0 ± 0.5	4.2 ± 3.1	0.7 ± 0.3	0.941	0.535	56
MeB	20	3.9 ± 1.4	4.4 ± 9.4	0.9 ± 0.9	0.895	0.541	17
	30	3.6 ± 0.2	5.9 ± 3.0	0.7 ± 0.2	0.988	0.150	204
	40	25.8 ± 593	0.1 ± 3.0	2.5 ± 6.3	0.956	0.395	21

$q_m$ : adsorption capacity;  $K_{\text{MLF}}$ : modified Langmuir-Freundlich constant the ( $n$ ) obtained at the studied temperatures;  $R^2$ : determination coefficient;  $\sigma^2$ : standard deviation fit;  $F$ : Fisher-Snedecor parameter; Mo1: Mordant Orange 1; RhB: Rhodamine B; MeB: Methylene Blue.

**Table 5.** Maximum adsorption capacities (Langmuir isotherm) of CFA for MeB and RhB

Dye	Adsorption capacity / ( $\text{mg g}^{-1}$ )	Temperature / °C	Reference
MeB	15.04	30	60
	0.07	30	53
	2.94	30	61
	5.57	30	62
	4.89	22	43
	3.98	30	this work
RhB	1.87	30	61
	5.03	22	43
	6.2	30	this work

RhB: Rhodamine B; MeB: Methylene Blue.

The thermodynamic parameters, Gibbs energy ( $\Delta G^\circ$ ), enthalpy ( $\Delta H^\circ$ ) and entropy ( $\Delta S^\circ$ ), can be calculated using equations 8 and 9.<sup>63,64</sup>

$$\Delta G^\circ = -RT \ln(K_L \times M_{\text{dye}}) \quad (8)$$

$$\ln(K_L \times M_{\text{dye}}) = \frac{\Delta S^\circ}{R} - \frac{\Delta H^\circ}{RT} \quad (9)$$

where  $R$  ( $8.314 \text{ J mol}^{-1} \text{ K}^{-1}$ ) is the ideal gas constant,  $T$  (K) the absolute temperature,  $K_L$  ( $\text{L mg}^{-1}$ ) the Langmuir

constant and  $M_{\text{dye}}$  the dye molar mass ( $\text{mg mmol}^{-1}$ ). The values of  $\Delta H^\circ$  and entropy  $\Delta S^\circ$ , were calculated from the slopes and intercepts of  $\ln(K_L M_{\text{dye}})$  versus  $1/T$  plot.

The calculated thermodynamic parameters for the adsorption of dyes under investigation are given in Table 6.

The negative  $\Delta G^\circ$  values for all temperatures indicate the spontaneous nature of the adsorption process. The negative values of  $\Delta H^\circ$  in MeB and Mo1 reveal that the adsorption reaction is exothermic meaning that the energy released by the new interactions between the dyes and solid is higher than the desorption of the solvent (water) molecules previously adsorbed, in the case of RhB the opposite is true since the process is endothermic.

The magnitude of  $\Delta H^\circ$  also allows to infer about the nature of the adsorption process. Literature describes that physical adsorption heat is in the same order of magnitude as the condensation heat, i.e., 2.1 to 21  $\text{kJ mol}^{-1}$ ,<sup>65</sup> while the chemisorption heats are in the range of 80 to 400  $\text{kJ mol}^{-1}$ .<sup>66</sup> Therefore, due to the relatively low  $\Delta H^\circ$  values in all the studied dyes it is expected that physisorption to be dominant. The positive value of  $\Delta S^\circ$  reflect an increase randomness at the solid/solution interface with some structural changes in the adsorbate and the adsorbent.<sup>67</sup>

Concerning the temperature effect directly on the maximum adsorption capacity, the decrease in MeB and

**Table 6.** Thermodynamic parameters for adsorption of dyes on CFA

Adsorbate	Temperature / °C	$\Delta G^\circ / (\text{kJ mol}^{-1})$	$\Delta H^\circ / (\text{kJ mol}^{-1})$	$\Delta S^\circ / (\text{kJ mol}^{-1} \text{ K}^{-1})$
Mo1	20	-23.019		
	30	-22.838	-12.835	0.030
	40	-22.113		
RhB	20	-33.908		
	30	-35.975	2.812	0.122
	40	-35.724		
MeB	20	-34.161		
	30	-34.791	-15.070	0.063
	40	-35.462		

$\Delta G^\circ$ : Gibbs energy;  $\Delta H^\circ$ : enthalpy;  $\Delta S^\circ$ : entropy; Mo1: Mordant Orange 1; RhB: Rhodamine B; MeB: Methylene Blue.

Mo1 may reflect the weakening of electrostatic interactions between dye molecules and active adsorbent sites with increasing temperature.<sup>68</sup> This effect may be compensated in the bulkier RhB molecule, which at higher temperatures has a higher diffusion rate.<sup>63</sup>

#### Effect of unburn carbon

One question when studying the coal fly ashes and their potential application as adsorbents is the relative importance of unburn carbon. This may be relevant when deciding to use the CFA without any treatment or increase their potential adsorption capacity through different physical or chemical treatments.<sup>69,70</sup>

A simple way to test the role of the carbon is trying to eliminate it through a thermal treatment. In this work, a calcination 555 °C was performed until the sample had constant weight. The adsorption capacity of this calcinated material was then tested for the Mo1 dye adsorption.

A direct comparison between the original and the calcinated CFA was made. Despite the difference between the original and calcinated CFA the application of the Langmuir model to the calcinated material ( $q_m = 108 \text{ mg g}^{-1}$ ,  $K_L = 0.013 \text{ L mg}^{-1}$ ) suggest that adsorption capacity is similar although less favorable for the calcinated sample, reflecting the slight influence of the carbon content in the original CFA.

#### Effect of solution pH

The solution pH is an important parameter influencing the adsorption capacity. The concentration of  $\text{H}^+$  affects the degree of ionization of the dye molecules as well as the surface properties of the adsorbent. In Figure 10 it is represented for Mo1 and MeB the effect of initial pH of the solution on the percentage of dye removed, at a fixed mass of CFA.

Results indicate that dye percentage removed is strongly influenced by the solution pH, in the case of Mo1 adsorption is favored in acid medium occurring a sharp adsorption decrease as the pH increases from 2 to 4. For MeB the adsorption is favored in basic media, this result has already been studied and justified. Some authors explain it using the concept of excess of hydronium ion competing with the cation groups on the dye for adsorption sites.<sup>71</sup> Other authors through the concept of change solid surface density and electrostatic repulsion.<sup>72</sup> Although a broader definition includes the  $\text{pH}_{\text{pzc}}$  effect, where the solid is positively charged at a pH lower than  $\text{pH}_{\text{pzc}}$  and negatively charged at a pH higher than  $\text{pH}_{\text{pzc}}$ .<sup>64</sup> It is possible to conclude that, in low values of pH, many positive charges exist in

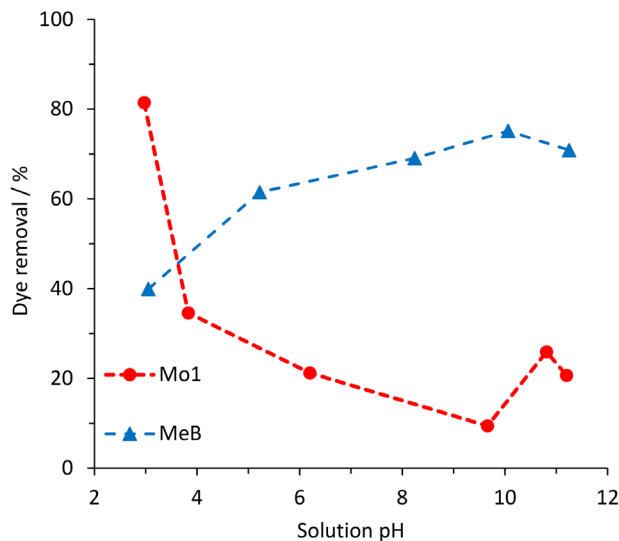


**Figure 10.** Dye removal percentage as a function of initial solution pH in a range of 2 to 12 for Mo1 and MeB dyes.

the CFA, which repel the cationic dye (MeB) and attract the anionic dye (Mo1). As the pH increases the positive charges decrease and so the correspondent repel/attraction effects also decrease until it reaches the CFA  $\text{pH}_{\text{pzc}}$  value of approximately 11, where the situation is inverted.

The pH effect may also explain the difference between the adsorption capacity CFA for the Mo1 and the other dyes in the model isotherm experiments. In order to simulate real conditions of operation the dye solutions were prepared without pH adjustment this meant that the initial pH for Mo1 solutions was around 5 and around 8 for RhB and MeB. At pH values lower than the  $\text{pH}_{\text{pzc}}$  the CFA surface should charge positively and increase the susceptibility to adsorb an anionic molecule like the Mo1.

## Conclusions

The purpose of this study was to explore the potentialities of residue such as coal fly ash, generated in coal-fired thermal powerplants, to be used without further treatment as an effective adsorbent to remove dyes from synthetic industrial wastewaters. The coal fly ash was physically and chemically characterized, and their inert behavior in aqueous media was demonstrated by no significant lixiviation effects. The textural characterization data show a low specific surface area when compared with traditional adsorbent materials such as activated carbon. Also, the microscopy images obtained suggest that the adsorption occurs mainly at the external surface of the ash particles. Results also showed that in non-adjusted pH solutions of Mo1 (anionic molecule) the adsorption is favored since  $\text{pH} < \text{pH}_{\text{pzc}}$  leading to a positively charged surface of the coal fly ash with adsorption capacities higher than

100 mg g<sup>-1</sup> in all temperature range. This effect was not observed with MeB and RhB dye molecules which are both cationic. In these cases, the adsorption capacities were around 4 to 6 mg g<sup>-1</sup> for MeB and RhB, respectively. The obtained results led us to conclude that the low specific surface area of CFA material (13.2 g m<sup>-2</sup>) has a small contribution on the dye adsorption phenomena. Instead, the adsorption capacity of CFA occurs mainly due to electrostatic interactions that are strongly dependent on the relation between the pH of the aqueous media and the surface chemistry of the CFA, quantified by its pH<sub>PZC</sub>. Despite the possibility of increasing adsorption capacity by simple modifications on the surface chemistry (i.e., oxidation), these treatments imply costs that should be evaluated according to each scenario.

## Acknowledgments

The authors wish to thank Central Termolétrica do Pêgo for CFA and the facilities to perform the characterization analysis. The authors also thank Prof Nuno Lapa from Departamento de Ciências e Tecnologia da Biomassa da FCT-UNL for the characterization assays of CFA and the fruitful discussion. This research was funded by Fundação para a Ciência e Tecnologia through UIDB/00100/2020 project of Centro de Química Estrutural.

## References

- Zhao, X.; Chen, H.; Liu, S.; Ye, X.; *Renewable Energy* **2020**, *157*, 695.
- Oberschelp, C.; Pfister, S.; Raptis, C. E.; Hellweg, S.; *Nat. Sustainable* **2019**, *2*, 113.
- GBD 2017 SDG Collaborators; *Lancet* **2018**, *392*, 2091.
- Yao, Z. T.; Ji, X. S.; Sarker, P. K.; Tang, J. H.; Ge, L. Q.; Xia, M. S.; Xi, Y. Q.; *Earth-Science Reviews* **2015**, *141*, 105.
- Ahmaruzzaman, M.; *Prog. Energy Combust. Sci.* **2010**, *36*, 327.
- Rashidi, N. A.; Yusup, S.; *ACS Sustainable Chem. Eng.* **2016**, *4*, 1870.
- Singer, A.; Berggaut, V.; *Environ. Sci. Technol.* **1995**, *29*, 1748.
- Joshi, R. C.; Lothia, R.; *Fly Ash in Concrete: Production, Properties and Uses*, vol. 2; Gordon and Breach Science Publishers: New York, USA, 1997.
- Iyer, R. S.; Scott, J. A.; *Resour., Conserv. Recycl.* **2001**, *31*, 217.
- Murayama, N.; Yoshida, S.; Takami, Y.; Yamamoto, H.; Shibata, J.; *Sep. Sci. Technol.* **2003**, *38*, 113.
- Tauanov, Z.; Azat, S.; Baibatyrova, A.; *Int. J. Coal Prep. Util.* **2020**, DOI: 10.1080/19392699.2020.1788545.
- Koshy, N.; Singh, D. N.; *J. Environ. Chem. Eng.* **2016**, *4*, 1460.
- Liu, Y.; Yan, C.; Zhao, J.; Zhang, Z.; Wang, H.; Zhou, S.; Wu, L.; *J. Cleaner Prod.* **2018**, *202*, 11.
- Feng, W.; Wan, Z.; Daniels, J.; Li, Z.; Xiao, G.; Yu, J.; Xu, D.; Guo, H.; Zhang, D.; May, E. F.; Li, G.; *J. Cleaner Prod.* **2018**, *202*, 390.
- Cheng, S. Y.; Liu, Y. Z.; Qi, G. S.; *Chem. Eng. J.* **2020**, *400*, 125946.
- He, X.; Yao, B.; Xia, Y.; Huang, H.; Gan, Y.; Zhang, W.; *Powder Technol.* **2020**, *367*, 40.
- Moreno-Castilla, C.; *Carbon* **2004**, *42*, 83.
- Martins, A.; Nunes, N.; *J. Chem. Educ.* **2015**, *92*, 143.
- Mittal, J.; *J. Environ. Manage.* **2021**, *295*, 113017.
- Soni, S.; Bajpai, P. K.; Mittal, J.; Arora, C.; *J. Mol. Liq.* **2020**, *314*, 113642.
- Mariyam, A.; Mittal, J.; Sakina, F.; Baker, R. T.; Sharma, A. K.; Mittal, A.; *Arabian J. Chem.* **2021**, *14*, 103186.
- Haddad, B.; Mittal, A.; Mittal, J.; Paolone, A.; Villemin, D.; Debtab, M.; Mimanne, G.; Habibi, A.; Hamidi, Z.; Boumediene, M.; Belarbi, E. habib; *Chem. Data Collect.* **2021**, *33*, 100717.
- Lu, G. Q.; Do, D. D.; *Fuel Process Technol.* **1991**, *27*, 95.
- Wee, J. H.; *Appl. Energy* **2013**, *106*, 143.
- Mushtaq, F.; Zahid, M.; Bhatti, I. A.; Nasir, S.; Hussain, T.; *J. Environ. Manage.* **2019**, *240*, 27.
- Kapoor, A.; Viraraghavan, T.; *Adsorpt. Sci. Technol.* **1992**, *9*, 130.
- Ochedi, F. O.; Liu, Y.; Hussain, A.; *J. Cleaner Prod.* **2020**, *267*, 122143.
- Zhu, L.; Ji, J.; Wang, S.; Xu, C.; Yang, K.; Xu, M.; *Chemosphere* **2018**, *206*, 278.
- Banerjee, S. S.; Jayaram, R. V.; Joshi, M. V.; *Sep. Sci. Technol.* **2003**, *38*, 1015.
- Huang, X.; Zhao, H.; Hu, X.; Liu, F.; Wang, L.; Zhao, X.; Gao, P.; Ji, P.; *J. Hazard. Mater.* **2020**, *392*, 122461.
- Viraraghavam, T.; Rao, G. A. K.; *J. Environ. Sci. Health, Part A: Environ. Sci. Eng. Toxicol.* **1991**, *26*, 721.
- Appiah-Hagan, E.; Chen, Y. W.; Yu, X.; Artega, G. A.; Pizarro, J.; Mercier, L.; Wei, Q.; Belzile, N.; *Simple and Energy-Saving Modifications of Coal Fly Ash to Remove Simultaneously Six Toxic Metal Cations from Mine Effluents*, vol. 6; Elsevier: London, UK, 2018.
- Joseph, I. V.; Tosheva, L.; Doyle, A. M.; *J. Environ. Chem. Eng.* **2020**, *8*, 103895.
- Chen, Y. W.; Yu, X.; Appiah-Hagan, E.; Pizarro, J.; Artega, G. A.; Mercier, L.; Wei, Q.; Belzile, N.; *Utilization of Coal Fly Ash and Drinking Water Sludge to Remove Anionic As(V), Cr(VI), Mo(VI) and Se(IV) from Mine Waters*, vol. 6; Elsevier: London, UK, 2018.
- Singh, V. N.; Chatuverdi, A. K.; Yadova, K. P.; *Water, Air, Soil Pollut.* **1990**, *9*, 51.
- Simha, P.; Ramanathan, A.; Thawani, B.; Jain, P.; Hussain, S.; Ganesapillai, M.; *Arabian J. Chem.* **2019**, *12*, 5049.
- Viraraghavam, T.; Alfaro, F. M.; *J. Hazard. Mater.* **1998**, *57*, 59.

38. Pura, S.; Atun, G.; *Sep. Sci. Technol.* **2009**, *44*, 75.
39. Chowdhury, M. F.; Khandaker, S.; Sarker, F.; Islam, A.; Rahman, M. T.; Aual, M. R.; *J. Mol. Liq.* **2020**, *318*, 114061.
40. Tiwari, D. P.; Singh, S. K.; Sharma, N.; *Appl. Water Sci.* **2015**, *5*, 81.
41. Astuti, W.; Chafidz, A.; Wahyuni, E. T.; Prasetya, A.; Bendiyasa, I. M.; Abasaed, A. E.; *J. Environ. Chem. Eng.* **2019**, *7*, 103262.
42. Kisku, G. C.; Markandeya; Shukla, S. P.; Sen Singh, D.; Murthy, R. C.; *Environ. Earth Sci.* **2015**, *74*, 1125.
43. Janoš, P.; Buchtová, H.; Rýznarová, M.; *Water Res.* **2003**, *37*, 4938.
44. ASTM D1762-84: *Standard Test Method for Chemical Analysis of Wood*, ASTM International, West Conshohocken, PA, 2007.
45. BS EN 15290: *Solid Biofuels, Determination of Major Elements, Al, Ca, Fe, Mg, P, K, Si, Na and Ti*, British Standards Institution (BSI), 2011.
46. EN 12457-2: *Characterisation of Waste Leaching Compliance Test for Leaching of Granular Waste Materials and Sludges Part 2: One Stage Batch Test at a Liquid to Solid Ratio of 10 l/kg for Materials with Particle size Below 4 mm (without or with Size Reduction)*, European Committee for Standardization (CEN), 2002.
47. Gregg, S. J.; Sing, K.; *Adsorption, Surface Area, and Porosity*, 2<sup>nd</sup> ed.; Academic Press: London, UK, 1982.
48. Prahas, D.; Kartika, Y.; Indraswati, N.; Ismadji, S.; *Chem. Eng. J.* **2008**, *140*, 32.
49. Özacar, M.; Şengil, I. A.; *J. Environ. Manage.* **2006**, *80*, 372.
50. Ho, Y. S.; McKay, G.; *Process Biochem.* **1999**, *34*, 451.
51. Kalembkiewicz, J.; Sitarz-Palczak, E.; *J. Ecol. Eng.* **2015**, *16*, 67.
52. Diário da República Eletrónico, <https://data.dre.pt/web/guest/legislacao-consolidada/-/lc/34518175/view?w=2020-12-10>, accessed in August 2021.
53. Karaca, H.; Altıntığ, E.; Türker, D.; Teker, M.; *J. Dispersion Sci. Technol.* **2018**, *39*, 1800.
54. Belviso, C.; *Prog. Energy Combust. Sci.* **2018**, *65*, 109.
55. Wang, S.; Boyjoo, Y.; Choueib, A.; Zhu, Z. H.; *Water Res.* **2005**, *39*, 129.
56. Jala, S.; Goyal, D.; *Bioresour. Technol.* **2006**, *97*, 1136.
57. Wdowin, M.; Franus, M.; Panek, R.; Badura, L.; Franus, W.; *Clean Technol. Environ. Policy* **2014**, *16*, 1217.
58. Langmuir, I.; *J. Am. Chem. Soc.* **1918**, *40*, 1361.
59. Ho, Y. S.; Chiang, C. C.; *Adsorption* **2001**, *7*, 139.
60. Hammond, C.; Padovan, D.; Tarantino, G.; *R. Soc. Open Sci.* **2018**, *5*, 171315.
61. Khan, T.; Ali, I.; Singh, V.; Sharma, S.; *J. Environ. Prot. Sci.* **2009**, *3*, 11.
62. Kumar, K. V.; Ramamurthi, V.; Sivanesan, S.; *J. Colloid Interface Sci.* **2005**, *284*, 14.
63. Ghosal, P. S.; Gupta, A. K.; *J. Mol. Liq.* **2017**, *225*, 137.
64. Liu, Q. S.; Zheng, T.; Wang, P.; Jiang, J. P.; Li, N.; *Chem. Eng. J.* **2010**, *157*, 348.
65. Smith, J. M. In *Chemical Engineering Kinetics*, 2<sup>nd</sup> ed.; Clark, B. J.; Kenter, S. A., eds.; McGraw-Hill: New York, USA, 1970.
66. Yu, Y.; Zhuang, Y. Y.; Wang, Z. H.; Qiu, M. Q.; *Chemosphere* **2004**, *54*, 425.
67. Mohan, D.; Singh, K. P.; Singh, G.; Kumar, K.; *Ind. Eng. Chem. Res.* **2002**, *41*, 3688.
68. Dogar, S.; Nayab, S.; Farooq, M. Q.; Said, A.; Kamran, R.; Duran, H.; Yameen, B.; *ACS Omega* **2020**, *5*, 15850.
69. Prado, P. F.; Nascimento, M.; Yokoyama, L.; Cunha, O. G. C.; *Am. J. Eng. Res.* **2017**, 394.
70. Xu, G.; Shi, X.; *Resour., Conserv. Recycl.* **2018**, *136*, 95.
71. Akkaya, G.; Güzel, F.; *Chem. Eng. Commun.* **2014**, *201*, 557.
72. Murugan, P.; Ramesh, S. T.; Biju, V. M.; *Sep. Sci. Technol.* **2020**, *55*, 471.

Submitted: May 25, 2021

Published online: August 17, 2021

